Physicochem. Probl. Miner. Process., 60(4), 2024, 192436

http://www.journalssystem.com/ppmp

Physicochemical Problems of Mineral Processing

ISSN 1643-1049

Production of pure tantalum and niobium oxides by hydrometallurgical processing of coltan smelter cake from Tanganyika Province/RD Congo using NH_4HF_2-KOH flux system

Bertin Kitungwa K.[1], Phalaris Yuma M.[1], Pierre Kalenga Mubiayi.[2], Michel Shengo L.[1], Grace Ngubeni.[2], Nosipho Moloto.[2], Marsi Mbayo K.[1], Crépin Kyona W.[1]

[1] Department of Chemistry, Faculty of Sciences, University of Lubumbashi, Haut-Katanga, DR Congo

[2] Faculty of Sciences, Molecular Science Institute, African Research University Alliance-Center of Excellence-Materials for Energy and Nanotechnology, University of Witwatersrand, Johannesburg, RSA

Corresponding authors: bertinokabuge@gmail.com (Bertin Kitungwa), Kalenga.Mubiayi@wits.ac.za (Pierre Kalenga)

Abstract: Pure tantalum and niobium oxides were produced from the molten cake after mixing ore-NH_4HF_2-KOH in a respective mass ratio of 1/4/3. This resulted in solubilization yields of over 95% for Nb and around 92% for Ta in sulfuric acid solution 3 molar. Extraction of tantalum and niobium using octan-2-ol yielded over 95% niobium and 98% tantalum when pH is set at 0.5-1.0 and 1.5-2 respectively. The compounds K_3NbOF_6, K_3NbO_4 and K_2TaF_7 were identified after melting. While in aqueous solution ionic species such as $NbF_6(OH)_2^{3-}$, NbF_6^- and $TaF_7^{2-}$are likely to be identified. Precipitation of tantalum and niobium in NH_4OH solution (pH=7.50-8.0) as hydrated oxides after stripping with distilled water and crystallization identified hydrated oxides such as $Ta_2O_5.nH_2O$, $Nb_2O_5.nH_2O$. These two oxides were associated with a small amount of $SiO_2.nH_2O$ as an impurity resulting from the extraction and precipitation of tantalum and niobium. SEM-EDS, XRD, TGA-DTG and FTIR analyses identified and characterized these compounds.

Keywords: Molten Coltan ore, ammonium bifluoride, potassium hydroxide, hydrometallurgical recovery of Ta and Nb, species identification

1. Introduction

Tantalum and niobium are essential metals sought for a variety of high-technological applications. The most recent studies have shown the possibility of leaching Ta and Nb in a mixture of hydrofluoric and sulfuric acid in a 6:1 ratio (Goitom, and Mulugeta, 2024). Treatment of tantalum and niobium solutions leads to the production of pure compounds. However, the use of highly corrosive acids, such as a mixture of hydrofluoric acid and sulfuric acid is the main drawback to consider besides cost implication, and environmental concerns associated with the method (Joson et al., 2016; El-Hussaini & Mohamed, 2002; Shikika et al., 2021). To circumvent this difficulty, many researchers propose an approach involving a melting step using molten salts (Nnaemeka, 2023; Zhou et al., 2005). Several combinations of fluxes have been proposed to reduce energy consumption (Wang et al., 2009) and to modify the mineralogical structure of tantalum and niobium (Kitungwa et al., 2020). For the past few decades, researchers have widely employed two approaches in using fluxes for modification of ore structure during smelting and for using the smelted product in water solubilization. The first approach proposes the use of alkaline hydroxides as fluxes (NaOH or KOH). This set of fluxes are part of , the first fusion method used on industrial scale (Wang et al., 2009; Habinshuti et al., 2022; Mona et al., 2019; Permana et al., 2016; Yang et al., 2012). The second approach proposes the use of ammonium bifluoride (NH_4HF_2) as a flux and this has been reported by several authors (Krysenk et al., 2016; Mpinga and Crousse, 2012; Nete et al., 2014; Purcell et al., 2018; Yan and Tang, 2018).

Alkali hydroxide (NaOH and KOH) and ammonium bifluoride (NH_4HF_2) fluxes are used to modify the mineralogical structure of the ore, yielding fused products that are soluble in water. The solubility of alkaline salts increases with their cationic radius, which would justify the increased use of caustic

DOI: 10.37190/ppmp/192436

potash as a flux in place of caustic soda (Kikuko, et al., 2021; Chunfu, et al., 2019). In the smelting approach, temperature remains a major challenging parameter during the beneficiation process of tantalum and niobium ores. To mitigate this challenge, our first approach was to combine the use of ammonium bifluoride and caustic potash in the same reactor during the smelting of coltan ore from Tanganyika Province in the south-east of the Democratic Republic of Congo (Kitungwa et al., 2020).

The combination of reagents during smelting was more beneficial as energy consumption during smelting, and water solubilization of tantalum and niobium. The advantage of this combination would the addition of KOH to the ore-NH_4HF_2 mixture already leading to an exothermic reaction whose heat release during the preparation of nearly 100 g of mixture can reach an average temperature of 120°C. This heat release promotes ore smelting even before treatment in the furnace. Optimum smelting was achieved at 160°C, with the ore/NH_4HF_2/KOH mass ratio of 1/4/3 respectively. This led to Ta and Nb having a solubility of 95% in water (Kitungwa et al., 2020). However, there are limitations such as the nature of the mineralogy of the tantalum and niobium sample, the different species formed in the products resulting from melting in the proposed mixture (NH_4HF_2-KOH), the nature of the water- and/or acid-soluble tantalum and niobium species.

The identification and characterization of these Ta and Nb species are important for understanding various chemical reactions and reaction mechanisms during melting the ore in NH_4HF_2-KOH mixture. The evaluation of conditions for solvent extraction of tantalum and niobium species by octan-2-ol from the aqueous solution resulting from the previous step (leaching of the melt cake) and their stripping according to the procedure proposed by (El-Hazek, et al., 2012; Mayorov and Nikolaev, 2002), followed by precipitation and the crystallization stages which will lead to the production of pure tantalum and niobium oxides.

2. Materials and methods

2.1. Materials

Various pieces of equipment were used to characterize the coltan ore sample. These included a 10 ml Brand graduated cylinder (Duran Germany, ISO 4788) for bulk density determination, a Boeco, Germany precision analytical balance, eight granulometric sieves (Jayant Scientific ind) with mesh sizes of 70µm, 100µm, 155µm, 212µm, 425µm, 600µm, 850µm and 1200µm (Kitungwa, et al., 2023; Habinshuti, et al., 2021). A Universal vibro-screening machine (Jayant Scientific ind) as well as different apparatus for conducting analyses: An X-ray Fluorescence spectrometer (XRF, branded thermo-scientific, Olympus), an optical microscope (branded Altion), a radiometer (branded Albert inspector), the X-ray Diffractometer (XRD, branded Vorsicht Röntgenstrahlung), two atomic emission spectrometers (ICP-OES branded Arcos and ICP-MS). The Scanning Electron Microscope coupled to the Electron Dispersion Spectrometer (SEM-EDS, branded Zeiss Sigma), Thermogravimetric analysis (TGA, branded PerkinElmer TGA 4000) and Fourier transform infrared (FTIR, branded FT-IR Nicolet Apex).

2.2. Methods

2.2.1. Coltan ore sample characterization

Coltan ore samples were collected from five active mining sites in Tanganyika province: Kisengo and Kahendwa in Nyunzu territory, Mayi-baridi in Kalemie territory, Ngobo and Dragon in Manono territory. All these territories are in Southeastern DR/Congo, approximately 500 km Northwest of the city of Lubumbashi (Wakenge, 2017).

First, physicochemical analyses were conducted. To determine the sample granulochemical characteristics, 1 kg of the coltan ore was passed over a series of sieves (from 1,200 µm to 70µm). The oversized particles retained by different sieves were shaken for 15 minutes, using a vibrating machine (Hadjersi, 1975). Nine granulometric fractions were obtained and subjected to XRF chemical analysis. The granulochemical distribution of tantalum and niobium was determined using equations (1) and (2) below:

$$\text{Oxide weight (g)} = \frac{\%\ \text{of oxide} \times \text{Weight in grams of screen rejects}}{100} \quad (1)$$

$$\text{Distribution (\%)} = \frac{\text{Mass of oxide on a given fraction} \times 100}{\text{Total mass of oxide on all particle sieves}} \quad (2)$$

The apparent density was determined by filling a 10 ml graduated cylinder with pulverized coltan ore and weighing the content this was calculated as the ratio of mass to volume of the sample (Yoro & Godo, 1990).

$$\text{Apparente density} = \text{Weight of sample in test tube/ Volume of sample in test tube} \quad (3)$$

Radioactivity of the coltan sample was determined by average of several measurements. Their mean value was corrected using results given by 800 grams of the material and compared to the background given by the measuring device (Euratom, 2012).

The loss on ignition was determined as the difference between the weight of the sample before and after calcination at 900°C.

$$\text{Fire loss (g)} = \text{WS}_{\text{bf}} - \text{WS}_{\text{af}} \quad (4)$$

with WS_{bf}: sample weight before calcination and WS_{af}: weight after calcination.

The mineralogical analysis was carried out samples deposited as thin film onto a substrate and studied using an optical microscope using with reflected and transmitted light.

2.2.2. Smelting of coltan ore and smelting product leaching

The smelting was conducted at 160°C in a 100 ml zirconium crucible for 60 minutes using a mixture including coltan ore, $NH_4HF_2$and KOH with $1/4/3$ as their respective mass ratios. The smelting product was characterized by SEM-EDS, XRD, and TGA analyses. The molten cake was solubilized in distilled water and in 3 molar sulfuric acid. Leaching yields were determined using the formulae 5, 6 and 7 :

$$\text{Y}_{\text{lix}}(\%) = (\text{W}_{\text{F}}/\text{W}_{\text{ES}}) \times 100\% \quad (5)$$

Where: $\text{Y}_{\text{lix}}(\%)$ is the leaching efficiency expressed in percent; W_{F} : the element weight (gram) in the filtrate and W_{ES} *the* element weight (gram) of in the sample. Knowing that:

$$\text{W}_{\text{F}} = [\text{C}_{\text{F}} \times \text{V}_{\text{F(ml)}}]/1000\text{ml} \quad (6)$$

and

$$\text{W}_{\text{EA}} = (\%_{\text{SA}} \times \text{W}_{\text{S}})/100 \quad (7)$$

with : C_{F} the element concentration (g/L) in the filtrate, V_{F} the filtrate volume (ml), $\%_{\text{SA}}$: percentage of an element in the sample, and W_{S} : the sample weight subjected to leaching.

2.2.3. Solvent extraction and stripping of tantalum and niobium

The acid leach solution and the water leach solution were mixed. The mixed solution was conditioned to pH values of 0.5, 1.0, 1.5, 2.0 and 2.5 for solvent extraction tests with octan-2-ol. The loaded organic phase was stripped with distilled water for tantalum and niobium recovery (El-Hazek, et al., 2012).

Solvent extraction was carried out for 5 minutes in separating funnels, stirring the mixture of organic and aqueous phases at a volume ratio of 1:1. After stirring, the cap of the separating funnel was opened to separate the phases. The loaded organic phase was mixed with distilled water to extract tantalum and niobium. The extraction yield was calculated using the following formula (8):

$$Y_{(\%)} = \frac{[\text{M}]\text{org.Vorg}}{[\text{M}].\text{Vorg}+[\text{M}].\text{Vaq}}\ x\ 100\% \quad (8)$$

where: $\text{Y}_{(\%)}$ is the metal extraction yield in percent, $[M]org$ and $[M]aq$ are the metal concentrations in the organic and aqueous phases, with $\text{V}_{\text{org}}$and V_{aq} the organic and aqueous phases volumes.

2.2.4. Precipitation and crystallization

Two types of solutions were used to precipitate tantalum and niobium as hydroxides, as per the procedure suggested by Mayorov and Nikolaev, (2002). NH_4OH served as the precipitant solution, in the pH range of 7.5 - 8.0 (El-Hazek, et al., 2012)**.** The precipitates obtained were subjected to crystallization through evaporation around 80°C-100°C (Ngoie and Kankolongo, 2022). The obtained crystals were identified using SEM-EDS, XRD, TGA-DTG, and FTIR analyses.

3. Results and discussion

3.1. Coltan ore characterization

The coltan ore characterization included chemical analysis, density and radioactivity measurement,

granulochemical, determination of the loss on ignition, mineralogical analysis, XRD, SEM-EDS, and TGA-DTG analysis.

3.1.1. Coltan ore chemical analysis, density, and radioactivity measurement

Results from the coltan ore density and radioactivity measurement are depicted in Table 1. Coltan ore mined in Tanganyika province has a bulk density of 6.181. This value falls within the density range characteristic of coltan ores (between 5.50 and 7.50). As for the radioactivity analysis, it gave an average value of 1651.6 Counts Per Minute (CPM) or 0.46 micro-sieverts per hour (μSv/h) for 800.00g of sample. The coltan ore from artisanal mines of Tanganyika province does not contain elements capable of endangering people through irradiation. It can therefore be handled or stored by artisanal miners, in compliance with the DR Congo law about protection against exposure to radioactive substances (Journal Officiel the DRC, 2005). The chemical composition of coltan ore mined in Tanganyika Province matches that of colombo-tantalite in which tantalum oxide (Ta_2O_5) presence prevails on that of niobium oxide (Nb_2O_5), that is 52% versus 41% (Kitungwa, et al., 2023; Habinshuti, et al., 2021).

Table 1. Coltan ore physicochemical and radioactivity analysis

Chemical elements	**Ta**	**Nb**	**Fe**	**Mn**	**Ti**	**Sn**	**Apparent density**	**Radioactivity for 800 grams of sample (μSv/h)**
Concentration (%)	28.11	24.46	3.55	7.13	0.32	2.21		
Chemical elements	**Si**	**Zr**	**Al**	**Ag**	**U**	**Th**	6.181	0.463
Concentration (%)	2.57	0.99	0.74	0.14	0.01	0.004		

3.1.2. Granulometrical analysis of coltan ore

Results from the granulochemical analysis of the coltan ore sample are depicted in Table 2. As can be seen from the results in Table 2, tantalum and niobium stand at 473.76 grams out of a total feed of 994.16 grams. Half of tantalum and niobium weight is made up of coarse particles with a size greater than 1200 μm whereas less than 10% of the total sample was found with the mineral particle size of 70μm. The ore sample grinding is necessary to liberate tantalum and niobium minerals and increase their specific area (contact surface) for better reaction at later processing stages. Consequently, the sample was subjected to grinding and sieving so to obtain 80% of particles less than 70 μm (El-Hussaini, 2002; Kitungwa, et al., 2023).

Table 2. Granulochemical distribution of coltan ore from Tanganyika

Size ranges (mm)	**Refusal weight (g)**	**Refusals weight percentage**	**Concentration (%)**		**Weight (g)**		**Distribution (%)**	
			Nb	**Ta**	**Nb**	**Ta**	**Nb**	**Ta**
1200	471.00	47.36	24.41	28.18	114.97	132.73	51.01	53.44
830	28.80	2.90	21.48	23.75	6.19	6.84	2.75	2.75
600	111.80	11.25	22.68	23.75	25.36	26.55	11.25	10.69
425	51.40	5.17	22.25	23.58	11.44	12.12	5.08	4.88
212	42.60	4.29	23.59	24.00	10.06	10.22	4.46	4.11
155	132.80	13.36	19.17	20.81	25.46	27.64	11.3	11.13
100	59.60	6.00	17.77	18.04	10.60	10.74	4.7	4.32
70	67.20	6.76	21.94	22.28	14.74	14.97	6.54	6.03
-70	28.96	2.91	22.65	26.15	6.56	6.57	2.91	2.65
Total	**994.16**	**100**			**225.38**	**248.38**	**100**	**100**

3.1.3. Coltan ore's content loss due to ignition

Calcining coltan ore in a 50 g crucible at 900°C resulted in a loss on ignition of around 0.484 g, or 0.968% of the total sample mass. This may be due to water loss from the sample's moisture content. It may also

result from the decomposition of organic matter during the calcination process, including loss of CO and CO_2.

3.1.4. Mineralogical analysis of coltan ore

Reflected-light optical microscopy of coltan ore (Fig. 1) identified tantalum and niobium oxides with color ranging from red to grayish, followed by cassiterite (tin oxide) with brown to yellow color, white iron oxides with a good polish, and blackish pyrolusite.

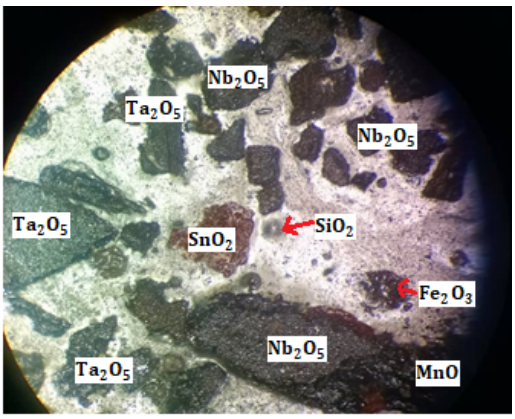

Fig. 1. Coltan ore image under a reflected-light optical microscope

3.1.5. Coltan ore analysis by XRD, SEM-EDS, and TGA-DTG

The coltan ore spectrum from analysis by EDS and its image from the Scanning Electron Microscope analysis (Fig. 2) match the results from the reflected-light optical microscope analysis. Indeed, they confirmed the presence of tantalum, niobium, iron, manganese, and tin oxides. Results from the chemical analysis using the X-ray Fluorescence spectrometer also supported it. The consistency between the obtained results was also established in terms of the intensity of the peaks given by the coltan ore analysis to the electron dispersion spectrometer. Tantalum peaks were more intense than those of niobium.

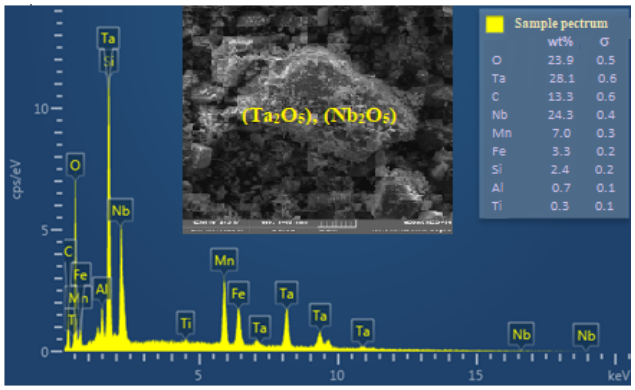

Fig. 2. SEM-EDS analysis of Tanganyika coltan ore

X-ray diffractometer (XRD) analysis of coltan ore under study (Fig. 3), before and after calcination, revealed the predominance of mineral oxides: $(Fe, Mn)(Ta, Nb)_2O_5$, Ta_2O_5, Nb_2O_5, SnO_2, MnO_2, $FeO(OH)$ and SiO_2. The calcination did not affect the sample structure. It increased the intensity of peaks about certain oxides. They include tantalum oxide represented by peak "a" and columbite-tantalite represented by peak "b", whereas for oxides such Nb_2O_5, SnO_2, and SiO_2, the intensity of peaks remained unchanged. Similar findings were reported by Wolf, et al., (2013) when they investigated the influence of temperature on tantalum oxide powder (Ta_2O_5). As confirmed the chemical analysis using X-ray fluorescence and mineralogical analysis by optical microscopy and the SEM-EDS-based methods (Kitungwa, et al., 2023), iron and manganese are among the major impurities found in coltan ore mined in Tanganyika province (Table 1).

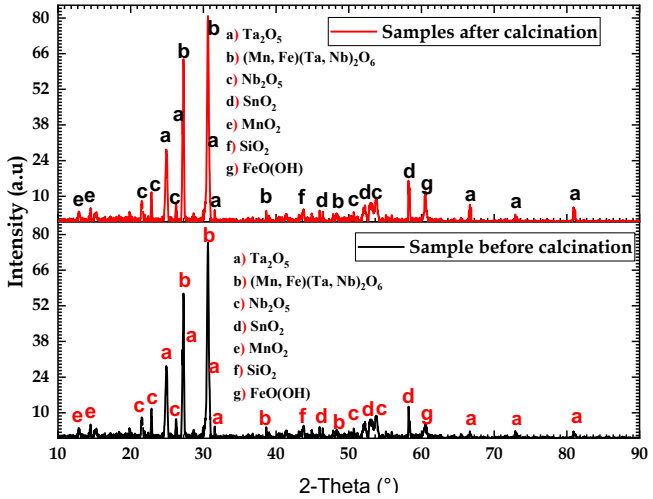

Fig. 3. XRD patterns of (top) calcined and (botom) uncalcined coltan sample

Thermogravimetric analysis (TGA) of coltan ore revealed three temperature-dependent stages (Fig. 4).

The first stage appeared between 152°C and 202°C and corresponded to a loss of 0.09%. This can result from water removal due to air humidity. As for the second stage, it appeared between 202°C and 364°C, with a loss of 0.528%. This can be attributed to the removal of amorphous carbon-bearing organic matter (Guanxu, et al., 2022). The third stage appeared between 364°C and 598°C, resulting in a loss of 0.346% versus the sample starting mass.

As for the Differential Thermogravimetry (DTG) curve, it revealed four endothermic bands. The first band appeared below 200°C while the second band appeared between 200°C and 300°C. This confirms the fixation of energy to eliminate water molecules. As for the third band, it appeared between 500°C and 600°C and resulted in the completed organic matter decomposition, including amorphous carbon as carbon monoxide (Taimur, et al., 2012). The endothermic band which appeared between 800°C and 900°C results from the elimination of intramolecular water in goethite (2 FeOOH) during its conversion into hématite (Fe_2O_3), under the effect of temperature (Gandon, 2021).

$$2FeOOH(s) \rightarrow Fe_2O_{3\,(s)} + H_2O(g) \tag{9}$$

Moreover, the TGA curve displayed very small slopes over the different temperature intervals, revealing the instability of produced intermediate compounds during the decomposition or removal of water molecules. Overall, the TGA and DTG curves revealed a mass loss of around 0.874%. This value is close to the one observed when determining the loss on ignition by subjecting the coltan ore sample to calcination (0.968%).

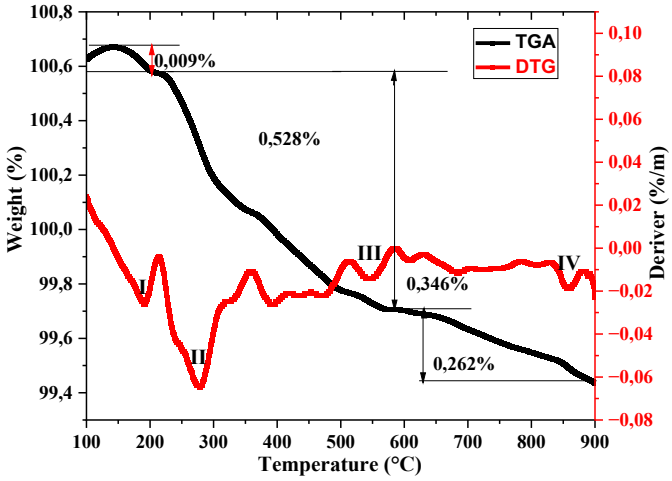

Fig. 4. Thermogravimetric (TGA) and differential thermogravimetric (DTG) analysis of the Tanganyika coltan sample

3.2. Coltan ore smelting, smelting cake leaching, and solvent extraction of tantalum and niobium

3.2.1. Coltan ore smelting using NH_4HF_2-KOH as flux

Based on results from previous studies carried out on the smelting of coltan, using NH_4HF_2 or KOH as flux, the reactions leading to smelting product formation can be identified as below:

- Melting in ammonium bifluoride NH_4HF_2 (Mpinga, 2013):

$$(Fe,Mn)(Ta,Nb)_2O_6(s) + 12NH_4HF_2\ (s) \rightarrow (NH_4)_2TaF_7(s) + (NH_4)(Fe,Mn)F_3(s) + (NH_4)_3NbOF_6 + 5H_2O(g) + 6NH_3(g) + 8HF \quad (10)$$

- Caustic potash melting KOH (Wang, et al., 2009):

$$(Fe,Mn)O(Ta,Nb)_2O_5(s) + 6KOH(s) \rightarrow 2K_3(Ta,Nb)O_4(s) + (Fe,Mn)O(s) + 3H_2O(g) \quad (11)$$

The smelting cake's mineralogical analysis by SEM-EDS (Fig. 5) showed that the coltan sample underwent modifications in its chemical composition (EDS) and morphology (SEM). This confirms that the coltan ore reacted in the presence of NH_4HF_2-KOH as flux, as seen through changes in the sample mineralogy. From the morphology standpoint, the smelting cake surface presented micropores which may be due to the release of gases. This confirms that the reaction between the ore-NH_4HF_2 mixture and KOH was exothermic (Kitungwa, et al., 2020). EDS image (Fig 5a) shows that melting coltan into the flux mixture leads to a decrease in metal concentration. This decrease in concentration is indicative of a new solution whose morphology is completely different (Fig 5b) from that recorded in Fig. 2.

The identification and characterization of species formed during the smelting of coltan ore in the NH_4HF_2-KOH mixture were done using XRD and TGA analysis (Figs. 6 and 7).

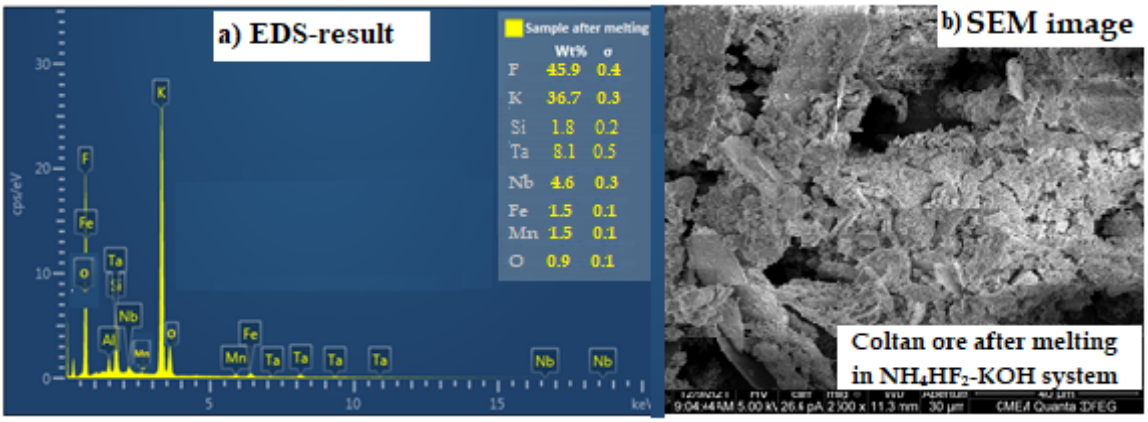

Fig. 5. SEM-EDS mineralogical analysis of coltan melts in NH_4HF_2-KOH mixture

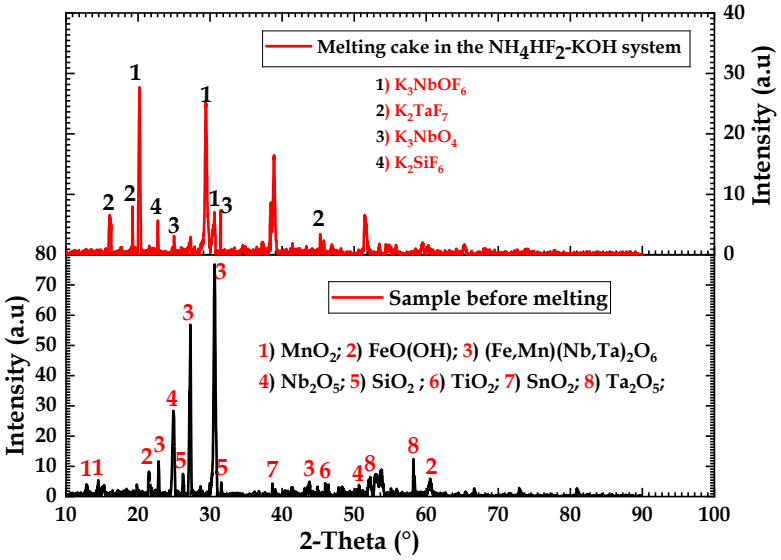

Fig. 6. XRD patterns of (top) melting cake in NH_4HF_2-KOH system and (bottom) coltan ore sample before melting

Analysis of the XRD diagrams (Fig. 6) reveals that smelting coltan ore in the presence of NH_4HF_2-KOH has resulted in changes affecting its mineralogical structure and morphology. Indeed, when comparing XRD patterns (2) and (1), one can notice the disapperance of some peaks including cassiterite (tin) peaks and a decrease in intensity of all peaks. This decrease reveals a drop in the concentration of metals in the melting cake due to mixing coltan ore with the two fluxes, as also shown by the EDS results (Fig. 5a). A thorough XRD analysis of peaks from of the smelting cake, reveals that four major compounds were likely to form during the smelting process of coltan ore, in the presence of NH_4HF_2-KOH. These are K_2TaF_7, K_3NbOF_6, K_3NbO_4 and K_2SiF_6 . The characteristic peaks of the first three compounds were also identified by (Netriová, et al., 2019; Ullha, et al., 2018).

Based on results from the mineralogical and chemical analysis of products from the smelting of coltan ore and leveraging from reaction mechanisms already suggested in the literature (Mpinga, 2013; Wang, et al., 2009), the smelting model of coltan ore can be predicted as one likely to occur as per the following reactions :

$$2Nb_2O_5(s) + 6NH_4HF_2(s) + 12\,KOH(s) \rightarrow 2K_3NbOF_6(s) + 2K_3NbO_4 + 6NH_3(g) + 12H_2O(g) \quad (12)$$

$$Ta_2O_5(s) + 7NH_4HF_2(s) + 10KOH(s) \rightarrow 2K_2TaF_7(s) + 2K_3TaO_4 + 7NH_3(g) + 12H_2O(g) \quad (13)$$

By considering the chemical compounds which were formed from reactions 12 and 13, it is also possible to envisage the formation of K_3TaOF_6under the same conditions as that of K_3NbOF_6 (Jianling, et al., 2008). In this case, two tantalum products (K_3TaOF_6 and K_3TaO_4) would also be likely to be identified when analyzing the melt cake using X-ray diffraction (Fig. 6), this is not the case. For K_3TaO_4, we did not find any characteristic peaks in the literature. On the other hand, the formation of K_2TaF_7 is evident in relation to the XRD results.

The results of the thermogravimetric analysis of the molten sample (Fig. 7) reveal three temperature steps similar to those obtained on the unmelted sample (Fig. 4). However, as the temperature increases, is significant in the case of the melt cake. A combined examination of the TGA and DTG results reveals only two very broad endothermic bands on the DTG curve, whereas four small bands were counted in the case of the unmelted sample (Fig. 4). The first endothermic band (Fig. 7) appears around 211°C and corresponds to the first temperature step between 159°C and 272°C on the TGA curve, with a mass reduction of around 4.56%. This reduction corresponds to the elimination of hydration water (Dávila, et al., 2021).

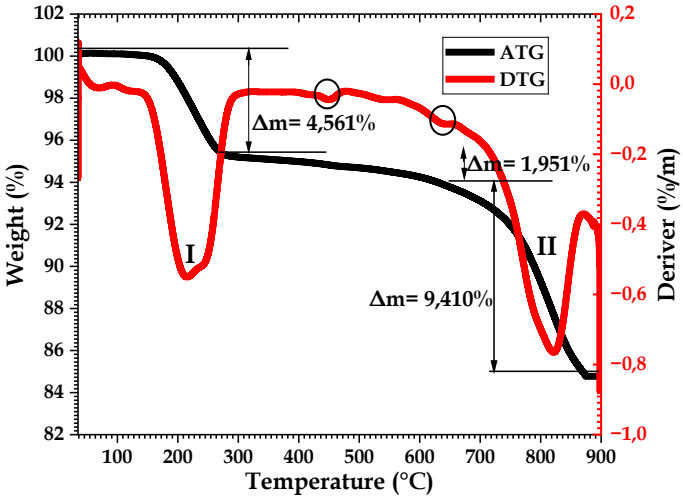

Fig. 7. Thermogravimetric analysis (TGA) and differential thermogravimetric analysis (DTG) curves of the melt cake

The second temperature plateau appeared between 272°C and 674°C. It corresponds to a mass reduction of around 1.95% on the TGA curve. Two small endothermic bands are visible in this temperature interval on the DTG curve. The first is indicated by a small black circle at 451°C. It corresponds to the decomposition of K_3NbOF_6 to NbO_2F, whose identification band appears at around 420°C in the results of (Rokov, and Mel'nichenko, 1984) and at around 400°C, (Wani, and Rao, 1991). The second is circled at 634°C and could be attributed to the decomposition of K_2SiF_6 into (2KF and

SiF_4) between 300°C and 700°C, the reaction of which occurs around 600°C (Verstraete et al., 2018).

$$K_3NbOF_6.H_2O(s) \leftrightarrow NbO_2F + 3KF(s) + 2HF(g) \quad (14)$$

During the smelting of coltan ore, K_2SiF_6 would be formed from the reaction of silica in the flux mixture, $NH_4HF_2 - KOH$ according to reaction (15) below:

$$3SiO_2(s) + 6NH_4HF_2(s) + 6KOH(s) \overset{\Delta}{\Leftrightarrow} 2K_2SiF_{6(s)} + K_2SiO_{3(s)} + 6NH_{3(g)} + 9H_2O_{(g)} \quad (15)$$

Finally, the third temperature range appeared between 674°C and 895°C with a mass decrease of around 9.41% and corresponds to the second endothermic band on the DTG curve. This could result from the decomposition of NbO_2F to Nb_3O_7F with the elimination of $NbOF_3(g)$ (Debachi, et al., 2017; Sten and Anders (1965) observed its decomposition reaction between 840°C and 970°C.

$$4NbO_2F_{(s)} \leftrightarrow Nb_3O_7F_{(s)} + NbOF_{3(g)} \quad (16)$$

3.2.2. Dissolution of tantalum and niobium through the smelting cake leaching

The yields of tantalum and niobium leaching in water and 3 molar sulfuric acid are indicative of the type of metal complexes that would be formed during coltan ore smelting in the NH_4HF_2-KOH flux mixture. The solubilization of coltan in water and sulfuric acid has given $NbOF_6(OH)_2^{3-}$, $Nb(OH)_5$ and $NbF_6^-(aq)$ as Nb-containing compounds; $TaF_7^{2-}$and $Ta(OH)_5$ are the main Ta-based complexes (Joson et al., 2016; Wang et al., 2009; Anatoly, 2004; Dávila, et al., 2021). In acidic media, the tantalum leaching yield increased to nearly 92%.

Table 3. Leaching yields of tantalum and niobium in two solvents

Used solvent	Corresponding leaching yields					
	Nb	Ta	Si	Sn	Fe	Mn
H_2O	94.19	71.98	84.88	81.20	22.46	23.12
H_2SO_4 : 3 molar	98.99	92.11	93.44	46.27	76.24	85.39

Taking into account the nature of the compounds formed during smelting in the proposed mixture (ore-NH_4HF_2-KOH), tantalum and niobium solutions would highlight the following reactions:

- Leaching with water as solvent:

$$K_3NbOF_6 + H_2O \rightarrow 3K^+ + NbF_6(OH)_2^{3-} \quad (17)$$

$$6K_3(Ta,Nb)O_4 + (5+n)\,H_2O \rightarrow K_8(Ta,Nb)_6O_{19}.nH_2O + 10KOH \quad (18)$$

- Leaching with sulfuric acid as solvent:

$$2K_2TaF_7 + 2H_2SO_4 \rightarrow 4H^+ + 2TaF_7^{2-} + 2K_2SO_4 \quad (19)$$

$$2K_3NbOF_6 + 3H_2SO_4 \rightarrow 2H^+ + 2NbF_6^- + 3K_2SO_4 + 2H_2O \quad (20)$$

$$2K_3(Ta,Nb)O_4 + 3H_2SO_4 + 2H_2O \rightarrow 2(Ta,Nb)(OH)_5 + 3K_2SO_4 \quad (21)$$

3.3. Solvent extraction of tantalum and niobium, precipitation and crystallization

3.3.1. Concentrations of major elements in leach liquors

Two types of leaching were carried out on the samples. Water leaching gave, almost all (95%) of the niobium solubilization compared with 71% for the tantalum. Leaching in 3-molar sulfuric acid allowed for solubilization of the tantalum to around 92% and 99% of the niobium (Table 3).

Chemical characterization (concentration in ppm and pH) of leaching solutions is presented in Table 4. The composite solution is made of mixture of the two leaching solutions, and the corresponding chemical contents and pH are found in the last line of the table.

Solubilization of tantalum and niobium in water and 3-molar sulfuric acid revealed that niobium solubilizes better than tantalum from the system NH_4HF_2-KOH. Looking at the pH value after leaching in water, it appears that the acidity of ammonium bifluoride dominates over the basicity of KOH. This implies that tantalum yields are better in the acid medium than in water (Tressaud, 2010). The main reason behind such solubilization is that two forms of tantalum compounds suggested are all acid-soluble, while only one is completely water-soluble.

Table 4. Elemental concentrations after leaching

Leach liquor	Chemical element concentration (ppm)						pH
	Nb	Ta	Si	Sn	Fe	Mn	
Water	4030	3283	1097	820	246	312	4.89
H_2SO_4 : 3 molar	4399	3949	1244	647	272	439	0.72
Composite solution	**4093**	**3497**	1129	713	246	366	**1.87**

3.3.2. Solvent extraction, precipitation and crystallization

The leaching solution was pre-conditioned for the solvent extraction step according to the procedure described in section 2.2.3, and the results are shown in Fig. 8.

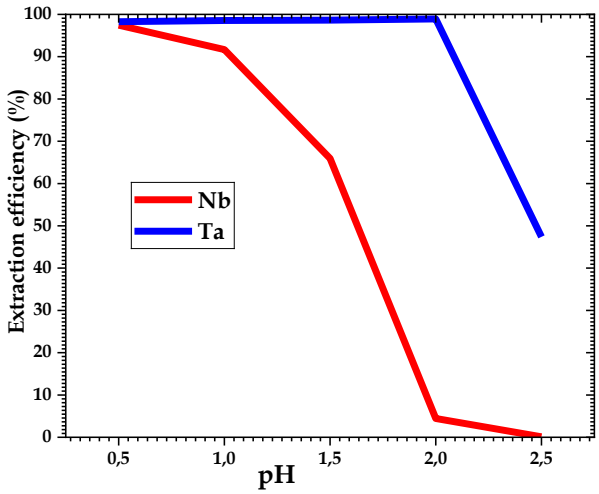

Fig. 8. Yield curves by Ta and Nb extraction with octan-2-ol as a function of pH

Tantalum extraction was better when pH increased in the range from 0.5 up to 2.5 (Fig. 8). Extraction yields of more than 98% were achieved in the pH range of 1.50-2.0. As for niobium, extraction yields decreased when the pH increased pH above 1.0. Hence, these metals differently behave during their solvent extraction as observed by other authors (El-Hazek, et al., 2012). It appears that the separation of these two metals can be achieved by readjusting the pH. Firstly, at pH= 2.0 to extract the Ta and secondly, bring the raffinate from the first extraction to pH = 0.5 to extract the Nb.

Based on the different forms of Ta and Nb in aqueous solution ($NbF_6(OH)_2^{3-}$, NbF_6^-, TaF_7^{2-}), the extraction, precipitation and crystallization reactions of these two metals can be described as follows :

For niobium**:** the form $NbF_6(OH)_2^{3-}$ must be transformed into NbF_6^- by lowering the pH of the solution:

1) Acidification of the solution:

$$NbF_6(OH)_2^{3-} + 2H^+ \leftrightarrow NbF_6^- + 2H_2O \quad (22)$$

2) Extraction with octan-2-ol ($\overline{OCL}$):

$$NbF_6^- + H^+ + \overline{OCL} \leftrightarrow HNbF_6 - \overline{OCL} \quad (23)$$

3) Stripping:

$$HNbF_6 - \overline{OCL} + H_2O \leftrightarrow NbOF_5^{2-} + 2H^+ + HF + \overline{OCL} \quad (24)$$

4) Precipitation and crystallization:

$$4H^+_{(aq)} + 2NbOF_{5\,(aq)}^{2-} + 10NH_4OH_{(aq)} \leftrightarrow Nb_2O_5.7H_2O_{(s)} + 10NH_4F_{(aq)} \quad (25)$$

$$Nb_2O_5.7H_2O_{(s)} \xrightarrow{\Delta} Nb_2O_{5(s)} + 7H_2O_{(g)} \quad (26)$$

For tantalum:

1) Extraction:

$$TaF_7^{2-} + 2H^+ + \overline{OCL} \leftrightarrow H_2TaF_7 - \overline{OCL} \quad (27)$$

2) Stripping:

$$H_2\mathrm{TaF}_7 - \overline{OCL} + 2H_2O \leftrightarrow TaF_7^{2-} + 2\mathrm{H}^+ + \overline{OCL} \quad (28)$$

3) Precipitation and crystallization:

$$4H^+_{(aq)} + 2TaF^{2-}_{7(\mathrm{aq})} + 14\mathrm{NH_4OH_{(aq)}} \leftrightarrow \mathrm{Ta_2O_5.9H_2}O_{(s)} + 14\mathrm{NH_4F_{(aq)}} \quad (29)$$

$$\mathrm{Ta_2O_5.9H_2}O_{(s)} \overset{\Delta}{\rightarrow} \mathrm{Ta_2O_{5(s)} + 9H_2O_{(g)}} \quad (30)$$

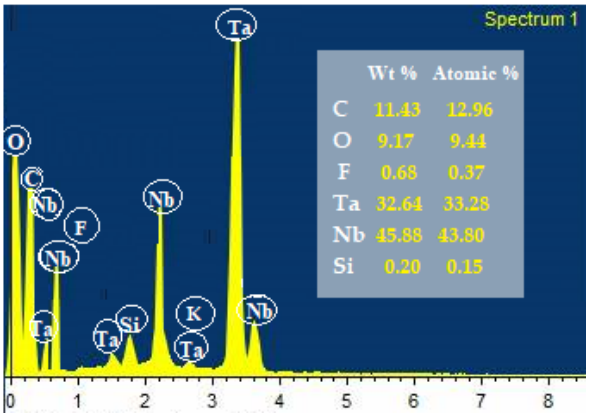

Fig. 9a. EDS spectrum of crystals from precipitation and crystallization of Ta and Nb solutions after extraction with octan-2-ol

SEM-EDS analyses (Figs. 9a and 9b) revealed the presence of tantalum oxide, niobium oxide, silicon and potassium fluoride after extraction by octan-2-ol. For the latter two elements, they may have not been extracted by octan-2-ol but, they were entrained in the organic phase during extraction and collected in the new aqueous phase after stripping. Analysis of the crystallographic forms (Fig. 9b) shows that tantalum and niobium produced oxides (Nb_2O_5 and Ta_2O_5) as identified by tetragonal and orthorhombic particles respectively. Whereas crystals in the form of solids white and powders that represent silica as well as potassium fluoride crystals (Huseynov, et al., 2015). The presence of fluorine is justified by the fact that the precipitation product was not washed with ethanol prior to the crystallization step. This is in line with the analysis of precipitation reactions number 25 and 29 above (Yuanyuan, et al., 2008).

The XRD analysis (Fig. 10) of crystals obtained from the precipitation of tantalum and niobium and crystallization of their precipitate revealed the presence of hydrated niobium and tantalum pentoxides ($Nb_2O_5.nH_2O$ and $Ta_2O_5.nH_2O$) (Barbosa & Castro, 2020) and silica ($SiO_2.nH_2O$).

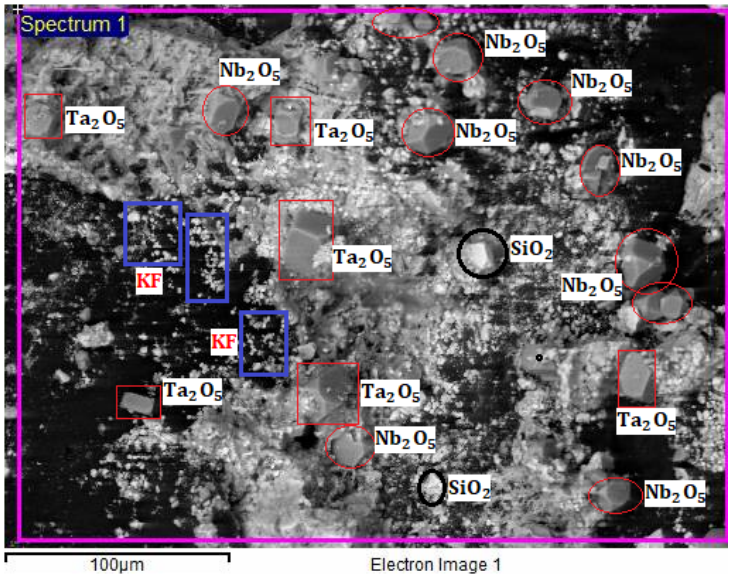

Fig. 9b. SEM of crystals from precipitation-crystallization of Ta and Nb solution after extraction with octan-2-ol

The TGA curve (Fig. 11) shows four temperature steps, with different compound mass losses, whereas the DTG curve presents two very broad and intense endothermic bands which are attributed to a temperature-induced decomposition of the product. The first and second stages of the TGA curve lie between 35°C and 90°C, and 90°C to 299°C, respectively. The first stage is associated with the first endothermic band, while the second stage is associated with the second endothermic band on the DTG curve. The first stage (I), with the endothermic band at 71°C, means evaporation of water through dehydration of tantalum and niobium oxides. Deblonde (2015) identified a mass loss of 9.40% at 85°C during the transformation of $Na_8(Ta_6O_{19}.24{,}5H_2O)$ into $Na_8(Ta_6O_{19}.15H_2O)$ whereas in this research a loss of 11.88% was observed at 71°C. This temperature is similar to that reported by Abramov in 2011 and by Beblonde (2015). In our case, the low dehydration temperature (71°C) would be justified by the presence of traces of fluorides.

The second stage (II) corresponds to a decomposition of KF already from 242°C up to 364°C. According to Wang, et al., (2016), this corresponds to its first decomposition stage. In this research, the endothermic band on the DTG curve is located around 272°C (temperature within the KF decomposition range). Above 300°C and up to around 800°C, the two curves TGA and DTG remained almost constant, with a plateau shape excluding any decomposition of the products formed (product stability zone). A new slope appeared between 800 and 900°C, the stability from the TGA and DTG curves of niobium oxide $Nb_2O_{5(s)}$ and tantalum $Ta_2O_{5(s)}$ above 850°C was also demonstrated by (Guanxu, et al., 2022; Wolf, et al., 2013).

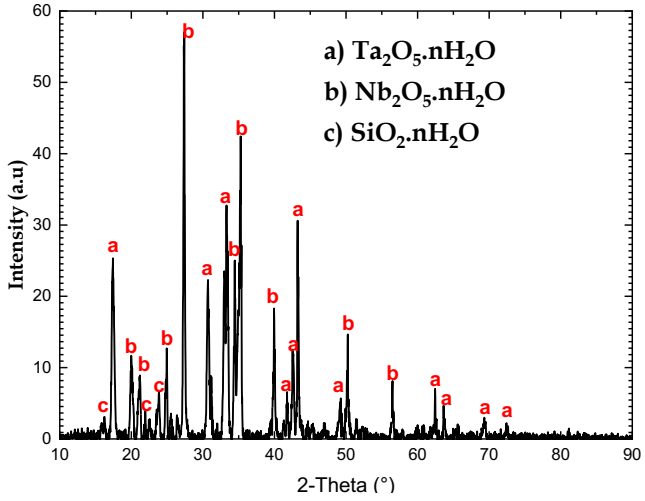

Fig. 10. XRD of sample from precipitation and crystallization of Ta and Nb solutions after extraction with octan-2-ol

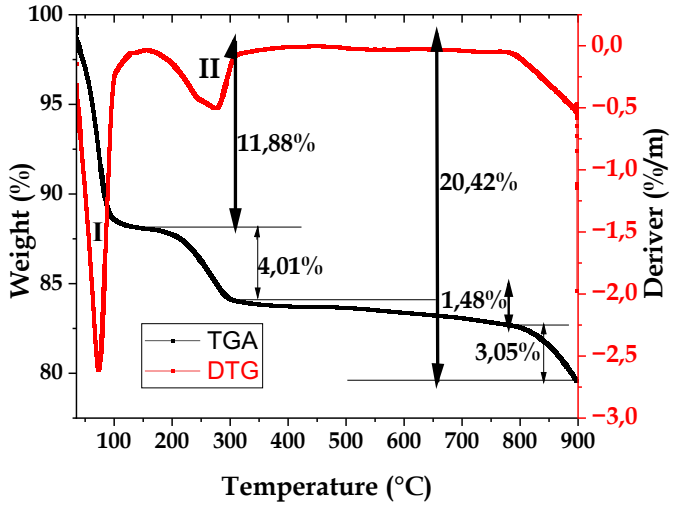

Fig. 11. TGA of crystals from precipitation-crystallization of Ta and Nb solutions after extraction with octan-2-ol

The finished product FTIR spectrum revealed ten infrared absorption bands (Fig. 12). This confirms that the product obtained is a mixture. In view of the results obtained, this mixture consists of hydrated oxides of Ta and Nb with silica as an impurity in this process (Zhang, Salje, & Ewing, 2002; Augsburger, et al., 2000; Jithin et al., 2021; Deshmukh, et al., 2012). Considering the complexity of FTIR bands obtained following the mixing of the final product, the major information that we can draw from this FTIR spectrum is the presence of a broad absorption band, which appears at a wavelength of 3290cm^{-1} due to the vibration of the OH (Hameed, Guerin, & Pierre, 2018). This band confirms the presence of water of hydration in the final product as we showed during the interpretation of the SEM-EDS, XRD and TGA-DTG results.

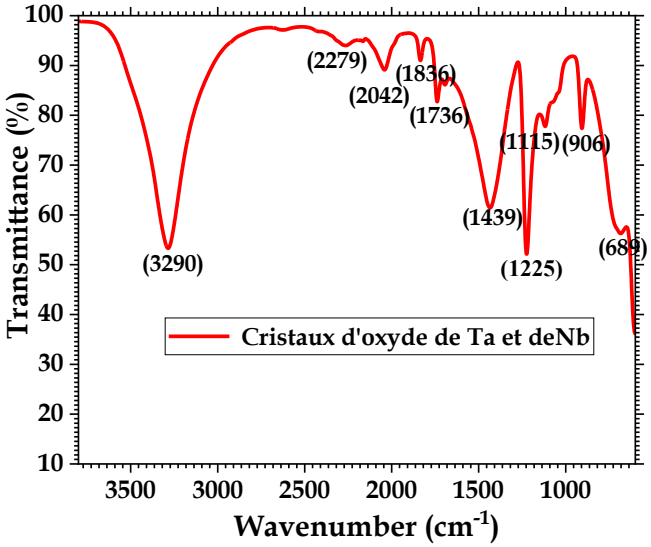

Fig. 12. FTIR of Ta and Nb crystals after precipitation-crystallization process of solution

4. Conclusions

The hydrometallurgical approach for production of pure tantalum and niobium oxides from the molten cake was studied in this research. Smelting at 160°C in the coltan ore mixture-NH_4HF_2-KOH (at a respective mass ratio of 1/4/3) produced, water- and acid-soluble Ta and Nb compounds. Compounds such as K_3NbOF_6 and $K_3(Ta,Nb)O_4$ and K_2TaF_7 were identified. The ions likely to form in aqueous solution are $NbOF_6^{3-}$, NbF_6^- and TaF_7^{2-}. This approach gave niobium leaching yields of over 95% and tantalum leaching yields of around 92%. Extraction with octan-2-ol as solvent enabled both metals to be collected at a pH between 0.50 and 1.0, with over 95% yield for niobium. pH of 1.5 to 2.0 allowed for an extraction yield of over 98% for tantalum. Characterization of the tantalum and niobium-based crystals revealed that hydrated niobium and tantalum oxides ($Nb_2O_5.nH_2O$ and $Ta_2O_5.nH_2O$) were produced.

Acknowledgments

The authors would like to thank the VLIR-UOS cooperation of Belgium with the University of Lubumbashi for the financial support that enabled us to carry out the analyses. We would also like to thank the Faculty of Sciences, Molecular Science Institute, African Research University Alliance-Center of Excellence-Materials for Energy and Nanotechnology, University of Witwatersrand, Johannesburg, RSA.

References

ALBERT, C., GEOFFREY, W., 1980. *Advanced Inorganic chemistry*, John Wiley and son. New York, 393-394, 752-765.

ANATOLY, A. (2004). *The chemistry of tantalum and niobium fluoride compound*. Amsterdam, The Netherlands, Netherlands: ELSEVIER Ltd.

AUGSBURGER, M.S., PEDREGOSA, J.C., SOSA, G.M., 2000. I*nfrared Spectroscopy and X-Ray Diffractometry Assessment of Order-Disorder in Oxide Minerals (Mn/Fe)(Nb/Ta)$_2$O$_6$*. Rev. Soc. Quím. Méx. Vol. 44, Núm.2.151-154.

BARBOSA , L., CASTRO, I., 2020. *Niobium-Titanium-Based Photocatalysts: Its Potentials for Free Cyanide Oxidation in Residual Aqueous Effluent*. Frontier in Chemistry, 1-11. doi:doi: 10.3389/fchem.2020.00099

CHUNFU, L., FANFEI M., LINGYUN L., JUN C., 2019. *Hydration properties of alkali and alkaline earth metal ions in aqueous solution: A molecular dynamics study*. Chemical Physics Letters, 727, *31–37.*

DÁVILA, LUISA F., QUINTERO, M.C., LONDOÑO, A.F., 2021. I*nfluence of synthesis process on the structural and microstructural behavior of neodymium-doped sodium and potassium niobate powders*. Journal of Physics: Conference Series, 2046 (2021) 012054, 1-6.

DEBACHI, J., BODY, M., GALVEN, C., BOUCHER, F., LEGEIN, C., 2017. *Preparation-Dependent composition anf O/F ordering in NbO_2F and TaO_2F*. Inorganic Chemistry, 56, 9, 5219-5232.

DEBLONDE, G. J., BENGIO, D., BELTRAMI, D., BÉLAIR, S., COTE, G., CHAGNES, A., 2019. *Niobium and tantalum processing in oxalic-nitric media: $Nb_2O_5 \cdot nH_2O$ and $Ta_2O_5 \cdot nH_2O$ precipitation with oxalates and nitrates recycling*. Separation and Purification Technology, Elsevier, 226, 209-217.

DEBONDE G., 2015. *Spéciation du niobium et du tantale en milieux basiques et développement d'un procédé hydrométallurgique pour la séparation niobium-tantale*. Thèse de Doctorat en Chimie physique et Analytique, 10-19, 79-84. Paris, France: Université Pierre et Marie Curie.

DESHMUKH, P., PESHWE, D., PATHAK, S., 2012. *FTIR and TGA analysis in relation with the % crystallinity of the SiO2 obtained by burning rice husk at various temperatures*. Advanced Materials Research Vol 585, 77-81.

EL-HAZEK, M., AMER , T., ABU , E.-A., ISSA, R., EL-HADY, S., 2012. *Liquid–liquid extraction of tantalum and niobium by octanol from sulfate leach liquor*. Arabian Journal of Chemistry, 5, 31-39.

EL-HUSSAINI, O., MOHAMED, M., 2002. *Sulfuric acid leaching of Kab Amiri niobium-tantalum bearing minerals, Central Eastern Desert, Egypt*. Hydrometallurgy, Elsevier,, 219-229.

EURATOM., 2012. *Proposition de directive du Conseil européen fixant les normes de base relatives à la protection sanitaire contre les dangers résultant de l'exposition aux rayonnements ionisants*. Chapitre II, article 4-92.

GANDON, A., 2021. *Élaboration de nanoparticules coeur@coquille magnétiques pour la catalyse de la scission oxydante des acides gras insaturés*. Thèse de Doctorat en génie chimique, 82-87. Québec, Canada: Université de Laval.

GOITOM, G., MULUGETA S., 2024. *Hydrometallurgical assessment of oxides of Nb, Ta, Th and U from Ethiopian tantalite ore*. Heliyon, Celpress, 1-9.

GUANXU , C., JINTAO , C., PROF. IVAN , P., DR. GUANJIE , H., DR. THOMAS , S., 2022. *Pseudohexagonal Nb_2O_5-Decorated Carbon Nanotubes as a High-Performance Composite Anode for Sodium Ion Batteries*. ChemElectroChem, European Chemical Societies publishing, 1-8.

HABINSHUTI, J., MUNGANYINKA, J. P., ADETUNJI, A. R., MISHRA, B., HIMANSHU, T., MUKIZA, J., ONWUALU, A. P., 2022. *Caustic potash assisted roasting of the Nigerian ferroferrocolumbite concentrate and guanidine carbonate-induced precipitation: A novel technique for extraction of Nb–Ta mixed-oxides*. Results in Engineering, Elsevier, 14, 1-13. doi:10.1016/j.rineng.2022.100415.

HABINSHUTI, J., MUNGANYINKA, J. P., ADETUNJI, A. R., MISHRA, B., HIMANSHU, T., MUKIZA, J., ONWUALU, A. P. OFORI-SARPONG, G., KOMADJA, G. C., 2021. *Mineralogical and physical studies of low-grade Tantalum-tin ores from selected areas of Rwanda*. Results in Engineering, Elsevier, 11, 1-11.

HADJERSI, Y., 1975. *Etude geostatistique du gisement de fer de Garadjebilet*. Projet de fin d'Etudes présenté à l'Université d'Alger, Ecole nationale de Polytechnique, Déparetement de Métallurgie, 1-89.

HAMEED, U., GUERIN, K., PIERRE, B., 2018. *Synthesis of Nb_2O_5 nanoplates and their conversion into NbO_2F nanoparticles by controlled fluorination with molecular fluorine*. European Journal of Inorganic Chemistry, 1-10.

HUSEYNOV, E., GARIBOV, A., MEHDIYEVA, R., 2015. *TEM and SEM study of nano SiO_2 particles exposed to the influence of neutron flux*. Journal Materials Research and Technology, 1-6.

IRMA LAMBERT and LAWRENCE H. CLEVER., 1992. *Solubility data series volume 52 alkaline earth hydroxides in water and aqueous solutions*. Pergamon Press. Oxford OX3 OBW, England. First edition 1992. Volume 52. 1-388.

JIANLING, Z., XIXIN, W., NING, L., 2008. *Ron Preparation and characterization of microsized $K_2Ta_2O_3F_6$ with ellipsoidal morphology by anodization*. Electrochemistry Communication, Elsevier, 10(2), 273–276.

JITHIN, P., SUDHEENDRAN, K., SANKARAN, K., KURIAN, J., 2021. *Influence of Fe-doping on the structural and photoluminescence properties and the band-gap narrowing of SnO_2 nanoparticles*. Optical Materials journal, Elsevier, 120, 1-15.

JOURNAL OFFICIEL DE LA RDC, 2005. Décret n° 05/019 du 29 septembre 2005 *portant organisation et fonctionnement du Comité National de Protection contre les Rayonnements Ionisants, en sigle* « C.N.P.R.I. », Article 6. Accessible via https://faolex.fao.org › docs › pdf › cng166324.

JOSON , Y., ARCOS, D., BOURGEOIS, F., BRUET, K., HÄKKINEN, A., ANDREIADIS, E., YE, G., 2016. *State-of-the-art on the recovery of refractory metals from primary resources*. Ref. Ares(2016)2234038, European Commission, MSP-REFRAM.

KIKUKO, H., YUSUKE, C., TOMOYUKI H., 2021. *Dynamic ionic radius of alkali metal ions in aqueous solution: a pulsed-field gradient NMR study*. Royal Society of Chemistry, RSC Advences, 11, 20252–20257.

KITUNGWA, B., YUMA, P., KATEULE, C., NTAMBWE, M. M., MBAYO, M., KYONA , C., 2023. *Physico-chemical and mineralogical characterization of coltan ores from the Tanganyika province in the Democratic Republic of Congo*.

KITUNGWA, B., YUMA, P., KATEULE, M., KYONA, C., WAKENGE, I., 2020. *Optimization of the water leaching parameters of tantalum and niobium contained in Manono ore in the Democratic Republic of Congo by fusion in the $NH4HF_2$-KOH system*. IOSR Journal of Applied Chemistry (IOSR-JAC)., 1-6.

KRYSENKO, G., EPOV, D., MEDKOV, M., MERKULOV, E., IVANNIKOV, S., NIKOLAEV, A., 2016. *Interaction of loparite concentrate with ammonium hydrodifluoride*. Russian Journal of Applied Chemistry, 89(4), 540-546. doi:doi:doi:10.1134/S1070427216040030

MAYOROV, V., NIKOLAEV, A., 2002. *Tantalum (V) and niobium (V) extraction by octanol*. Hydrometallurgy, Elsevier, 66, 77-83.

MONA, N., NAWAL, H., AZZA , A., 2019. *Potash Breakdown of Poly-Mineralized Niobium-Tantalum-Lanthanides Ore Material*. American Journal of Analytical Chemistry, 10, 103-111. doi:doi:DOI: 10.4236/ajac.2019.103009

MPINGA , K., CROUSSE , P., 2012. *Separation of niobium and tantalum from Mozambican tantalite by ammonium bifluoride digestion and octanol solvent extraction.* Hydrometallurgy, 129-130, 151-155. doi:doi:doi:10.1016/j.hydromet.2012.06.008

MPINGA K., 2013. *Extraction and separation of tantalum and niobium from Mozambican tantalite by solvent extraction in the ammonium bifluoride-octanol system*. Dissertation submitted in partial fulfillment of the requirements for the degree of MSc (applied science),. Thesis, 21-22. Department of Chemical Technology, University of Pretoria, South Africa.

NETE, M., PURCELL, W., NEL, J., 2014. *Separation and isolation of tantalum and niobium from tantalite using solvent extraction and ion exchange*. Hydrometallurgy, 149, 31-40.

NETRIOVÁ, Z., BOČA, M., DANIELIK, V., MIKŠÍKOVÁ, E., 2019. *Phase diagram of the system KF-K_2TaF_7-Ta_2O_5*. Journal of Thermal Analysis and Calorimetry, 95(1), 111-115.

NGOIE, P., KANKOLONGO R., 2022. *Evaluation des conditions de production des cristaux de sulfate de cobalt après extraction par solvant dans le système D_2EHPA-cyanex 272.* Mémoire de Bachelier en Sciences Chimiques, Faculté des Sciences, Université de Lubumbashi, Inédit. Lubumbashi, RD Congo.

NNAEMEKA S., 2023. *Pyrometallurgical Approach in the recovery of niobium and tantalum*. Intech-open, 1-23.

PERMANA, S., SOEDARSONO, J., RUSTANDI, A., MAKSUM, A., 2016. *Other oxides pre-removed from Bangka tin slag to produce a high-grade tantalum and niobium oxides concentrate.* IOP Conference Series: Materials Science and Engineering, 1-9.

PURCELL, W., POTGIETER, H., NETE, M., & MNCULWANE, H., 2018. *Possible methodology for niobium, tantalum, and scandium separation in ferrocolumbite.* Minerals Engineering, 119, 1-25.

ROKOV, E., MEL'NICHENKO, E., 1984. *The properties and reactions of ammonium fluorides*. Russian Chemical Reviews, 53(9), 859-869.

SHIKIKA, A., MUVUNDJA, F., MUGUMAODERHA , M., GAYDARDZHIEV, S., 2021. *Extraction of Nb and Ta from a coltan ore from South Kivu in the DRC by alkaline roasting thermodynamic and Kinetic aspects.* Minerals Engineering, 1-11.

SHIKIKA, A., SETHURAJAN, M., MUVUNDJA, F., MUGUMAODERHA, M.C., GAYDARDZHIEV ST., 2020. *A review on extractive metallurgy of tantalum and niobium*. Hydrometallurgy, Elsevier, 198 (105496), 1-13.

STEN , A., ANDERS , A. 1965. T*he thermal decomposition of NbO_2F*. Acta chemica Scandinavica, 19, 2136-2138.

TAIMUR , A., AMEED , H., ALI , H., ZUBAIDA , A., ANSARI, S., 2012. *One-Pot Synthesis and Characterization of Nb_2O_5 Nanopowde*. Journal of Nanoscience and Nanotechnology, 12, 7922–7926.

TRESSAUD, A., 2010. *Functionalized inorganic fluorides: synthesis, characterization & properties of nanostructured solids*. United Kingdom: Wiley J., & Sons, the Atrium, Southern Gate.

ULLAH, S., ULLAH, I., IQBAL, Y., MANAN, A., ALI, S., KHAN, A., 2018. *Influence of P_2O_5 and SiO_2 addition on the phase, microstructure, and electrical properties of $KNbO_3$*. Iran Journal of Sciences and Technology, 1-6.

VARTIKA, S., & MOHARIL , S., 2020. *Synthesis and Characterization of K2SiF6 Hexafluorosilicate. IOP Conf. Series: Materials Science and Engineering*., 1-7. doi:doi:10.1088/1757-899X/1104/1/012004.

VERSTRAETE, R., SIJBOM, H. F., JOOS, J., KORTHOUT, K., POELMAN, D., DETAVERNIER, C., SMET, P., 2018. *Red Mn4+-doped fluoride phosphors: why purity matters.* ACS Applied Materials & Interfaces, 10(22), 1-20.

WAKENGE, I., 2017. *Stadium coltan, Artisanal Mining, Reforms and Social Change in Eastern Democratic Republic of Congo.* Thesis submitted in fulfillment of the requirements for the degree of doctor at Wageningen University. The Netherlands.

WANG, X., ZHENG, S., XU, H., ZHANG, Y., 2009. *Leaching niobium and tantalum from a low-grade ore using a KOH roast–water leach system*. Hydrometallurgy. Elsevier, 219-223.

WANI, B., RAO, U. (1991). *Mode of thermal decomposition of $(NH_4)_3NbOF_6 \cdot 1.5H_2O$.* Thermochimica Acta, 176, 203–207.

WOLF, M., ROITSCH, S., MAYER, J., NIJMEIJER, A., BOUWMEESTER, H., 2013. *Fabrication of ultrathin films of Ta_2O_5 by a sol-gel method*. Thin Solid Films journal, Elsevier., 354-357.

YAN, H., TANG, D., 2018. T*echnical Features and Research Progress of Separating Impurities in Producing Tantalum (Niobium) Oxide by Traditional Technology*. International Journal of Mineral Processing and Extractive Metallurgy, 3(2), 29-36.

YANG, X. L., WANG, H. X., WEI, C., ZHENG, L. S., ZHANG, Y., 2012. D*ecomposition behaviors of tantalum-niobium ore in sodium hydroxide system.* Advanced Materials Research., 644-649.

YORO , G., GODO, G., 1990. *Les méthodes de mesure de la densité apparente: Analyse de la dispersion des résultats dans un horizon donné*. Cah. ORSTOM, Sér. Pédol., XXV(4), 423-429.

YUANYUAN, Z., ZIFENG, Q., MENGKAI, L., AIYU, Z., QIAN, M., 2008. *Preparation and characterization of porous Nb_2O_5 nanoparticles*. Materials Research Bulletin, Elsevier, *43*, 1363–1368.

ZHANG, M., SALJE, E. K., EWING, R., 2002. *Infrared spectra of Si–O overtones, hydrous species, and U ions in metamict zircon: radiation damage and recrystallization*. Journal of Physics: condensed matter, 14, 3333–3352.

ZHOU, H., ZHENG, S., ZHANG, Y., 2005. *Leaching of a low-grade niobium-tantalum ore by highly concentrated caustic potash solution*. Hydrometallurgy. Elsevier., 1-7.